Proceedings of ERAD (2002): 305–311 © Copernicus GmbH 2002

ERAD 2002

Ground clutter characterization and elimination in mountainous terrain

M. Gabella and R. Notarpietro

Politecnico di Torino, Electronics Department, Corso Duca degli Abruzzi, 24, 10129 Turin (Italy)

Abstract. A simple and fast texture-based technique for the removal of residual ground clutter is presented. Its main advantages are that it is easy to implement (both for polar and Cartesian data) and can be applied *a posteriori* after any other method of clutter removal has been applied. The performances of the technique during clear-sky and rainy conditions are analyzed for a 180×150 km^2 complex-orography region, using data from a non-Doppler and a Doppler radar (for both, approximately 50% of the clear-sky clutter shows average reflectivity greater than 13 dBZ). In the case of the non-Doppler data, the texture-based code is used after a prestored static map: it is absolutely necessary and leads to excellent results. In the case of the Doppler data, the technique can be applied with satisfactory results, even after a recent approach, which, in addition to a Doppler velocity test, combine all the available information concerning radar echoes.

1 Introduction

Ground echo is a challenge for weather radar data analysis, particularly as far as hydrology and precipitation estimates are concerned: because of ground clutter, precipitation accumulation algorithms perform inconsistently when heavy or extended clutter is present. Elimination of ground clutter is a prerequisite for the use of weather radar, both for quantitative and qualitative purposes. Since European radars are often in charge of the surveillance of a complex-orography region, they are from necessity installed on the top of a hill or a mountain. There, the rejection of clutter becomes of vital importance, since a clear view from a high site implies a large number of ground clutter pixels. A simple solution for clutter elimination is the use of a static clutter map, determined from a series of radar images in clear sky conditions (e.g. an average ground clutter map).

The large and rapid-short term fluctuations of clutter pose a serious problem in the choice of the "rejection-threshold": during extensive measurements with a non-Doppler C-band radar, we have found that a threshold that is 3.5 dB larger than the mean ground clutter cross section, eliminates 90% of the ground clutter echoes, regardless of its distribution. Often the distribution of time-varying clutter echoes can be fitted, by using one of the following distributions: Rayleigh (independent randomly distributed scatterers, e.g. Wallace, 1953), Rice (a dominant scatterer within many Rayleigh scatterers, e.g. Ker, 1987), lognormal (e.g. Linell, 1966) and Weibull (e.g. Boothe, 1969). For these skewed-to-the-right distributions, the ratio of the average to median is smaller than 1.6 dB (Rice), equal to 1.6 dB or larger than 1.6 dB (Weibull and lognormal, typical values are often about 5-10 dB). The drawback of the static map method is obviously residual clutter and the loss of considerable valid precipitation (a compromise that depends on the value of the selected value of the threshold).

A more efficient technique for removing the effect of ground clutter is to detect and abandon the echo signal contaminated by the ground clutter (Geotis and Silver, 1976). In this context, the use of high range resolution radar gates ($<$100 m) and Doppler velocity information, maximizes the probability of having at least some clutter-free radar bins for each pixel of the Cartesian operational product. A sophisticated and efficient approach that combine all the information available concerning radar return is the decision tree algorithm, combined with an adaptive clutter map, as proposed by Joss and Lee (1995) (hereafter referred to as JL95) and implemented at all the sites of the MeteoSwiss radar network (Joss et al., 1998). This signal-processing algorithm is not simply based on Moving Target Indicator technology, but rather on a decision-tree classification system that takes a clutter/non-clutter decision for each 83 m raw gate. The algorithm uses the Doppler (radial) component of the target velocity, the spectrum width, the minimum detectable signal, one-lag and two-lag signal fluctuations, and the vertical gradient of reflectivity as well as a continuously updated "occurrence" clutter map.

This map contains a counter for each radar gate, which is

Correspondence to: M. Gabella (gabella@polito.it)

updated by each conclusive choice made within the decision-tree classification system, but which is only consulted when none of the decisions in the tree has been conclusive. Being dynamic, this adaptive clutter map contains far fewer blind spots than its static counterpart, since the counter is usually saturated at twelve and, as a consequence, it reflects only current clutter and not an integration of daily or monthly amounts.

A simple texture-based elimination algorithm, that is particularly effective for the rejection of residual ground clutter, is presented in Sect. 2. Structure simplicity and short simulation times were pursued as primary goals during the planning phase: it is easy to implement (both for polar and Cartesian data) and can be applied *a posteriori*, after any other available method of clutter removal has been used. The two C-band radars, whose data are used to assess the texture-based code, are presented in Sect. 3. The mountainous region where the two non-collocated radars are found and, in particular, the 180×150 km^2 case study area, are described in Sect. 4. The texture-based performances in clear-sky (Sect. 5) and rainy (Sect. 6) conditions are then discussed, as well as other innovative and efficient methods of clutter removal.

2 Texture-based algorithm for the removal of residual clutter and anomalously propagated echoes

The algorithm is based on the fact that non-stationary ground clutter and anomalously propagated echoes (anaprop) decorrelate rapidly in space and are spatially heterogeneous to a great degree. Their signatures may be recognized in reflectivity data, as their spatial variability is larger than the weather echoes. The technique focuses on the horizontal spatial variability of the radar reflectivity field. Hence, it should be applied only to reflectivity data with the same altitude. However, it will be seen that it is effective even when applied to reflectivity data that do not strictly belong to the same height (e.g. maximum reflectivity maps). The algorithm is divided into two parts: the first part is a "spatial-proximity" filter and the second is a test of compactness. The former is a consequence of the larger spatial continuity of precipitation fields than ground clutter, and the latter of the different area/perimeter characteristics of residual clutter and anaprop with respect to precipitation fields.

The "spatial-continuity" filter that is applied to each pixel eliminates data that are weakly spatially correlated to the surrounding ones. For this purpose, we chose to place a 5×5 pixel window around the considered pixel (or bin, if polar reflectivity data are analyzed); its value is assumed to be a meteorological echo when the differences between it and n_p surrounding pixels in the 5×5 window are below a certain threshold tr_{var}; otherwise, the pixel is considered to be affected by ground clutter and a flag replaces its value. The choice of tr_{var} should be based on tools, which are able to quantify the spatial continuity of the precipitation fields through the analysis of their multiscale statistical properties (e.g. spatial Fourier power spectra, generalized structure function, moment-scale analysis, see Harris et al., 2001). In the present study, the choice is based on the variogram-based study by Germann and Joss (2001), who found that at ∼1 km lag (n_p = 8, that is, 8 surrounding pixels with ∼1 km distance) even a (1-hour) Mesoscale Convective System in the Alps has an average variance of no larger than 6 dBZ. The choice of a 5×5 window seems to be a good compromise: a 3×3 window is too selective while a larger one would filter too weakly. Also, the selection of $tr1$ and np can obviously influence the clutter removal process. However, the choice of thresholds within an "acceptable" range (3 dBZ $\leq tr1 \leq$ 9 dBZ, $6 \leq n_p \leq 10$) does not drastically change the results of the filtering algorithm.

The second part of the algorithm identifies adjacent pixels of not null intensity: the pixels are considered to belong to the same group if they touch on any of the eight possible directions (including diagonal directions). The ratio R of the total number of pixels in the group and the number of pixels defining its boundary is evaluated for each group. It has been verified in a number of radar maps that residual clutter groups often have a ratio R close to 1. Thus, choosing a threshold level $tr2$ slightly greater than one, will eliminate most of the unwanted clutter. Very small thunderstorm cells, with a medium life of about half an hour and a lateral extension of a few square kilometers can, unfortunately, be removed by this procedure. A choice of $tr2$=1.3 has been made for this second threshold. This value implies that the smallest "compact" group accepted as a meteorological feature must have more than 11 pixels.

3 Instrumentation description

The C-band, non-Doppler radar ($Bric$) was the first digital operational system installed in Italy (both the antenna and the sensor have recently been upgraded). At the time of the experiment, the 1.54° beam were averaged over four range-bins of 250 m and resampled on a Cartesian kilometric grid. A projection of the maximum reflectivity value over the entire columnar volume was generated every 5 min. The C-band, Doppler radar ($Lema$) was the first "new generation" radar to be installed by MeteoSwiss. The specifications were the consequence of decades of work with radars similar to the $Bric$ one. The full volume is scanned in 5 min with a 1° beam (20 elevations). It is accomplished in two cycles with interleaved elevation angles, each cycle lasting 2.5 minutes. Each range-bin is the average of a maximum of 33 gates, which have 83 m range resolution: the JL95 clutter elimination algorithm presented in Sect. 1 and implemented at the radar site takes a clutter/non-clutter decision for each 83 m raw gate. The 1°×1°×80 m "JL95-clutter-free" range bins are averaged and resampled on a Cartesian grid. Unfortunately, reflectivity values with the JL95 elimination algorithm disabled are not operationally available; only "JL95-clutter-free" pixels are stored. In this study, all the 5-min maximum reflectivity maps of the two radars have been post-processed using the texture-based algorithm presented in Sect. 2.

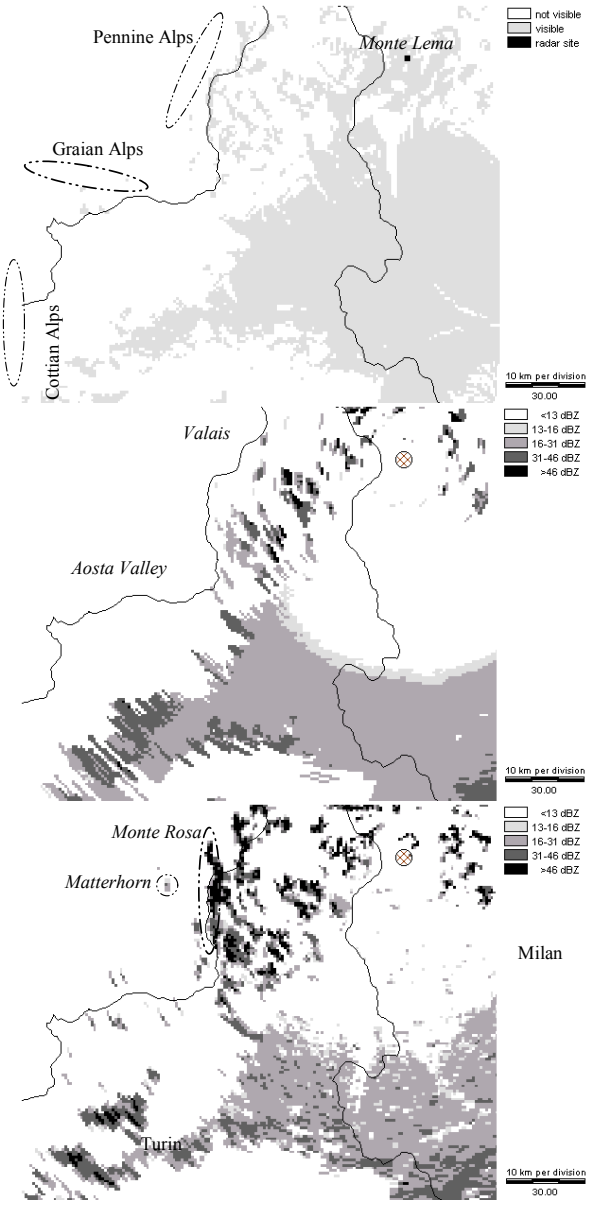

Fig. 1. Top: pixels in view from the *Monte Lema* radar site. Center: simulated clear-sky ground clutter map. Bottom: observed clear-sky ground clutter map at 13:15 UTC, 17 April 1997. The three pictures refer to a (R_{eq}/R_{earth} = 1.25) atmospheric refractivity profile.

4 Description of the case study area

In the present study, the effectiveness of ground clutter elimination is quantitatively assessed on a common 180×150 km^2 complex-orography area located in the North-West part of Italy. It is a partly flat and partly hilly area surrounded by very high mountains (the Alps) in the northern and western parts (see e.g. Fig. 1 of Gabella et al. in this volume for a map of the region). The Doppler radar is located on the top of *Monte Lema* at 1625 m a.s.l. The non-Doppler radar is located on the top of the *Bric della Croce* peak at 710 m a.s.l., just 5 km East of Turin.

A first-order, rough, "ground clutter characterization" of the two radar sites is quite straightforward and can easily be derived by computing the number of visible pixels using a simple geometric-optics approach. Assuming a standard refractivity gradient (the equivalent-earth's-radius used in the simulation stages is 1.25 times that of the real value) and using a Digital Elevation Map with 1×1 km spatial resolution, we find (e.g. for the Lema radar) the pattern shown in Fig. 1: approximately 38% of the pixels are in view from the Lema site (from the Bric site $\sim$35% of the 180×150 pixels are in view). The possibility of having ground clutter contamination increases even more if we extend the analysis to the south (non-shielded flat lands) and discharge the shielded areas (*Aosta Valley, Valais*): within the Piedmont region (whose political boundaries are represented by a black line), 56% of the pixels are visible from $Bric$ and 59% from $Lema$. The figures are obviously different for the northern lands, where there is considerable shielding by topography: the number of visible pixels in a 400×400 km$^\circ$ area around the Lema radar site is approximately 25%. Not only visible pixels (geometric optics approach) but also shielded areas contribute to ground clutter: for a more precise estimate of shadowing effects, the diffraction theory should be used where the geometric optics theory predicts zero illumination (Doviak and Zrnic, 1985). This procedure would be extremely time consuming and eventually impossible, because of the lack of details in the DEM and of the refractive index structure (ray tracing).

If one is interested in characterizing C-band ground clutter above a "rainy-threshold" (e.g. 13 dBZ), then the geometric optics approach is sufficient: the "rainy-threshold" cuts off most of the echoes that originate from diffraction and also several near-by, "weak-echo" pixels illuminated only by the radar beam secondary lobes. This effect is clearly visible in the central picture of Fig. 1, which shows ground clutter echoes with "equivalent" reflectivity, Z, larger than 13 dBZ, as simulated by a computer code for radar site assessment that, in its simplest version, requires only a raster Digital Elevation Map, the radar parameters and an estimate of the mean atmospheric refraction (Gabella and Perona, 1998). With almost-standard refractivity condition (equivalent Earth's Radius, R_{eq}, set to 1.25), the number of pixels with an equivalent echo stronger than drizzle ($Z > 13$ dBZ) is 29% of the selected area, almost the same as a real observation. The bottom picture in Fig. 1 shows ground

Clutter power as measured by the Lema radar on 17 April 1997 at 13:15 UTC (clear-sky condition). The measured pattern shows more small-scale variations in clutter intensity that can be reduced by averaging several maps (some of them are also caused by the presence of urban areas that are not inserted in the backscattering model). However, the agreement between the simulation and the observation is acceptable for the first 3 classes. The simulation considerably underestimates the number of echoes larger than 46 dBZ: only a hundred instead of about 6 hundred pixels have been observed.

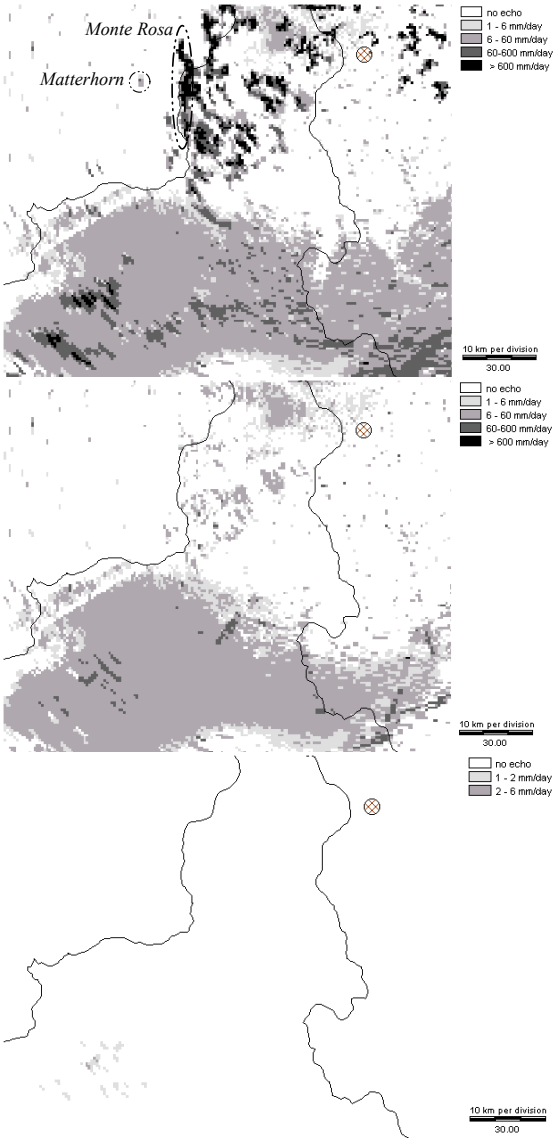

Fig. 2. "Equivalent" daily amount of rain on a clear-sky day (28 September 1996). Top: no clutter rejection. Center: Joss and Lee (1995) algorithm (JL95). Bottom: JL95 plus the texture-based algorithm presented in Sect. 2.

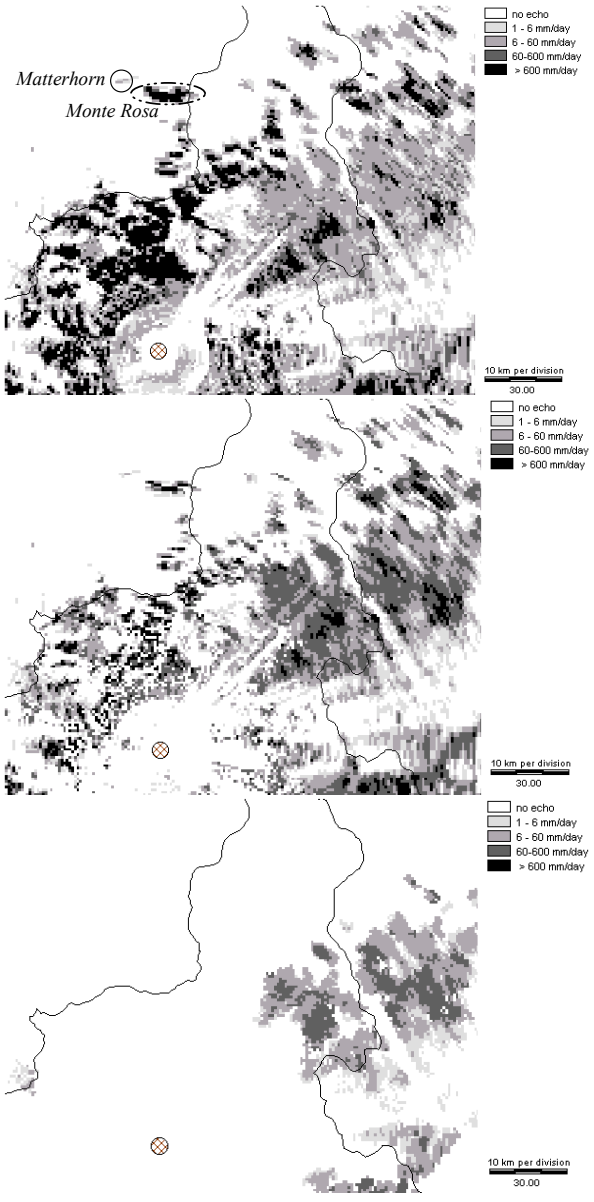

Fig. 3. Equivalent daily amount of rain, as derived from clear-sky clutter echoes for the non-Doppler ($Bric$) radar on 28 September 1996 (at 00:00 UTC the measured atmospheric refractivity was R_{eq}/R_{earth} = 1.47, same as in Fig. 2). Top: no clutter rejection. Center: static map (the threshold used was the median daily cross-section). Bottom: static map plus texture- based algorithm presented in Sect. 2.

5 Clear-Sky conditions post-processing

In this section, the daily average pattern of ground clutter during clear-sky standard refractivity conditions is presented for both radar systems. The effectiveness of the texture-based clutter elimination algorithm is clearly shown by comparing daily averages of treated and not-treated maps. The results refer to an average of 288 maximum reflectivity maps acquired by both radars on 28 September 1996. The radio sounding that is available from Milan at 12:00 UTC, shows quasi-standard decreases of refractivity (defined as the amount that the air refraction index (in parts per million) exceeds the value in vacuum and measured using the so-called N_{units}) in the lower atmosphere. The refractivity gradient (-50 N_{units}/km) was slightly larger than the usual one (-30 N_{units}/km). This larger than usual bending of electromagnetic rays causes a larger than usual pattern of ground clutter (see e.g. Fig. 1, for comparison). Figure 2 shows the equivalent daily amount of rain, as derived from clear-sky clutter echoes for the Doppler Monte Lema radar. The top picture shows the average ground clutter returns with-

out any kind of clutter rejection (this image is the average of just a few maps "extrapolated on a daily basis", since, as previously explained, maps of reflectivity with the elimination algorithm disabled are, unfortunately, not available). As expected, many pixels (∼50%) show values larger than 1 mm/day, while values larger than 600 mm/day are 2.3% of the 27 000 km^2 area. The central picture shows the effectiveness of the JL95 algorithm: 39% of the pixels now exceed the 1 mm/day threshold and, most of all, the average intensity has significantly decreased. Only 2 neighboring pixels belong to the largest class. It is still worthwhile to post-process the 288 maps with the texture-based algorithm (lower picture): at the end, only 0.3% of the pixels exceed 1 mm/day (a weaker class has been added so as to avoid showing an almost completely white picture).

Figure 3 shows the daily average of clutter echoes for the non-Doppler $Bric$ radar. The situation is similar to that of the $Lema$ site for the case of no clutter rejection. Part of the clutter can be eliminated even with the static map technique (central picture, the threshold used in this example was the median daily cross-section). The texture-based post-processing leads to a considerable improvement: 14% of the pixels show daily average values larger than 6 mm/day and no pixels larger than 600 mm/day. Most of the echoes are "permanent" (they occur in all the 288 maps that are available in a day). Table 1 summarizes the algorithm performances in clear-sky conditions.

6 Rainy conditions post-processing

6.1 Historical Doppler and non-Doppler data

To consider that all the cluttered pixels during fine weather are invisible during precipitation is obviously too pessimistic and, certainly, overrates the role of clutter. According to our experience, to consider that all the weather echoes that are weaker than the average clear-sky signals are hidden by ground clutter is certainly conservative, perhaps even pessimistic. We have always observed a general decrease of permanent clutter returns during rainy conditions.

Figure 4 shows the performances of the texture-based algorithm during rainy conditions (29 June 1997) when applied *a posteriori* after other clutter rejection techniques. The maps show, for each pixel, the equivalent daily amount of precipitation that has been identified as clutter by the texture-based algorithm. In other words, each picture shows the difference between two daily maps like those displayed in the center and bottom part of Figs. 2 and 3 (but derived using 288 maps acquired in rainy conditions): the top picture, in fact, refers to (the $Bric$ radar) non Doppler data, after the use of a simple pre-stored static clutter map (set to the median value); the central picture refers to (the $Lema$ radar) Doppler data, after the JL95 operational decision-tree clutter elimination algorithm.

By comparing these patterns with clear-sky patterns (Figs. 2 and 3), we can conclude that it is extremely likely that the texture code was successful in identifying these echoes as clutter. We can also conclude that the texture-based post-processing is completely efficient (and necessary) after the simple static map method and still beneficial even after the more sophisticated approach (JL95) that has been implemented by MeteoSwiss.

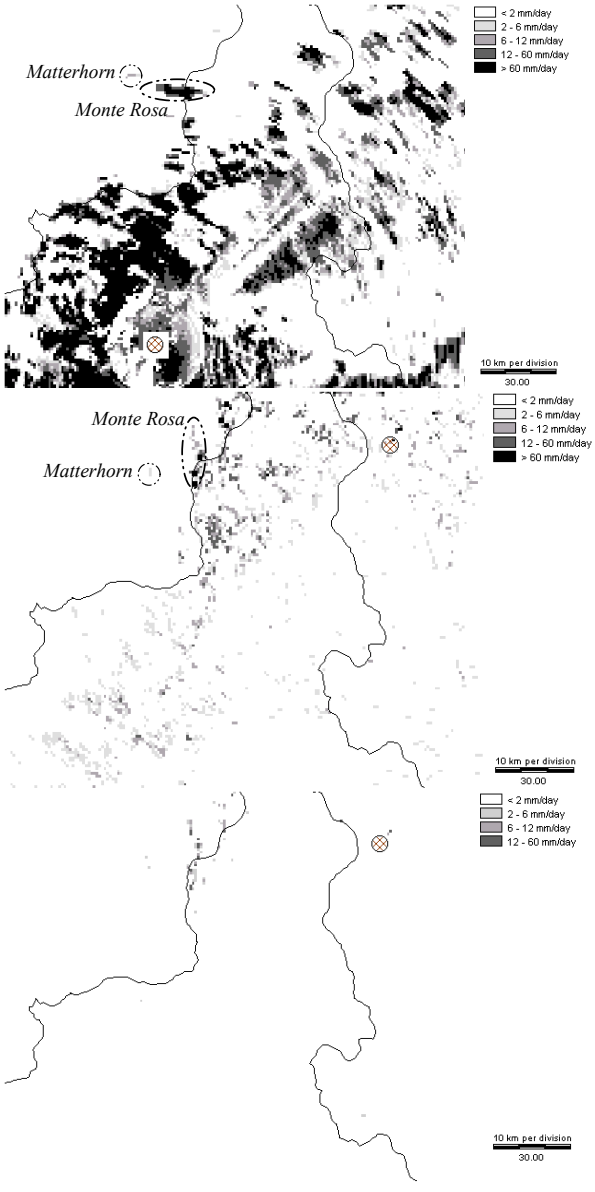

Fig. 4. Residual daily amount of ground clutter detected by the texture-based code when applied after other operational method of clutter removal in strong rainy condition. Top: non-Doppler radar. Centre: Doppler radar with JL95 algorithm. Bottom: Doppler radar with modified JL95 (Germann and Joss 2002). The first two pictures refer to 29 June 1997. The last picture to 14 October 2000.

Table 1. Texture-based clear sky performances when applied after other operational methods of clutter removal, namely the static map (non-Doppler $Bric$ radar) or the Joss and Lee (1995) algorithm (Doppler radar)

Type of clutter elimination	Percentage of clutter cells resulting in daily amount of rain			
	greater than $Bric$ radar	**1 mm/day** $Lema$ radar (Doppler)	**greater** than $Bric$ radar	**600 mm/day** $Lema$ radar (Doppler)
None	48%	50%	9.0%	2.3%
Operational	38%	39%	3.3%	0.01%
Operational + Texture	14%	0.3%	No pixel	No pixel

6.2 Recent data (after "state of the art" elimination)

Several experiments were performed at MeteoSwiss in 1998 and 1999 to further improve the efficient operational algorithm of the Swiss radar network. A modified version of the JL95 algorithm (see Sect. 2.3 of Germann and Joss 2002) was implemented in summer 1999 (hereafter referred to as GJ2002). Residual clutter was successfully reduced further. This is shown in the bottom picture of Fig. 5: the daily equivalent amount of precipitation identified as clutter by the texture-based algorithm on a recent rainy day (e.g. 14 October 2000) has further decreased. We have interpreted this fact as a consequence of a more effective clutter rejection by the modified version of the JL95 algorithm.

7 Summary and conclusions

The performances of a simple and fast texture algorithm for residual clutter removal during clear-sky and rainy conditions have been analyzed in a 180×150 km^2 complex-orography region, using data from two non-collocated C-band radar: a non-Doppler radar and a Doppler one. During clear-sky conditions, we have found that:

- for both radar sites, the number of pixels that exhibit a daily equivalent amount of rain larger than 1 mm/day is about 50% of the whole area ($\sim$13 500 km^2);
- concerning the non-Doppler radar, the use of a static map reduces the areal extent from 50% to 38%, while the combined use of a static map and a texture code reduces it to 14%;
- concerning the non-Doppler radar, the operational MeteoSwiss algorithm (JL95) alone reduces the areal extent of echoes larger than 600 mm/day from 2.3% to 0.01% of the whole area (namely 2 km^2);
- the combined use of the operational JL95 algorithm plus the texture code, reduces the areal extent of clear-sky ground clutter returns larger than 1 mm/day from 50% to 0.3%. After the texture-based post-processing, no more pixels show amounts larger than 6 mm/day.

During rainy conditions, we have found that the post-processing texture-based code successfully reduced residual clutter left not only by the static map technique, but also by the JL95 algorithm and its improved version (GJ2002); we have interpreted the fact that the amount of clutter identified by the texture-code after the static map was much larger than after JL95 (which, in turn was larger than GJ2002) as further proof that the JL95 algorithm is much better than a simple static map and, in turn, that its recent modified version, GJ2002, is better than the original one. In short, we can conclude that the texture-based post-processing clutter elimination here presented is particularly efficient (and necessary) after e.g. a simple static map method and no-Doppler filtering. It is also beneficial after the more sophisticated (JL95) approach implemented by MeteoSwiss, even in its recent optimised form (GJ2002). We plan to assess the efficiency of the texture-based code also after widely used Doppler-based elimination techniques like Moving Target Indicator (pulse pair) or FFT-based filters.

References

Boothe, R.R, The Weibull distribution applied to the ground clutter backscatter coefficient, Tech. Rep. No. RE-69-15, U.S. Army Missile Command, Redstone Arsenal, AL, 1969.

Doviak R.J., and Zrnic, D.S., Siting of Doppler weather radars to shield ground targets, IEEE Trans. on Ant. and Prop., 33, 685-689, 1985.

Gabella, M., and Perona G., Simulation of the orographic influence on weather radar using a geometric-optics approach, J. Atm. Oc. Tech., 15, 1486-1495, 1998.

Geotis S.G., and Silver, W.M., An evaluation of techniques for automatic ground-echo rejection, Preprints, 17th Conf. Radar Meteorology, Seattle, WA, Amer. Meteor. Soc., 448-452, 1976.

Germann, U., and Joss, J., Variograms of radar reflectivity to describe the spatial continuity of alpine precipitation, J. Appl. Meteor., 40, 1042-1059, 2001.

Germann, U., and Joss, J., Operational measurement of precipitation in mountainous terrain, In: Advanced Applications of Weather Radar, edited by P. Meischner. Chapter 2, Springer Verlag. In Press, 2002.

Harris, D., Foufoula-Georgiou, E., Droegemeier, K.K., and Levit, J.J., Multiscale statistical properties of a high-resolution precipitation forecast, J. Hydrometeorology, 2, 406-418, 2001.

Joss, J., and Lee, R., The application of radar-gauge comparisons to operational precipitation profile corrections, J. Appl. Meteorol., 34, 2612-2630, 1995.

Joss, J., and Coauthors, Operational use of radar for precipitation measurements in Switzerland, Vdf Hochschulverlag AG an der ETH Zürich, 108 pp., 1998.

Kerr, D.E., Propagation of short radio waves. Peregrinus Ltd., London, UK, 1987.

Linell, T., An experimental investigation of the amplitude distribution of radar terrain return, 6th Conf. of the Swedish National Committee on Scientific Radio, 1966.

Wallace, P.R., Interpretation of the fluctuating echoes from randomly distributed scatterres, part II, Can. J. Phys., 31, 995-1009, 1953.